Geology, geochemistry and geochronology of the Songwe Hill carbonatite, Malawi

Sam Broom-Fendley[1]*, Aoife E. Brady[2,6], Matthew S.A. Horstwood[3], Alan Woolley[4], James Mtegha[2], Frances Wall[1], Will Dawes[2] and Gus Gunn[5]

[1]Camborne School of Mines, University of Exeter, Penryn Campus, Cornwall, TR10 9FE, United Kingdom

[2]Mkango Resources Ltd., 259 Windermere Road SW, Calgary, Alberta, T3C 3L2, Canada

[3]NERC Isotope Geosciences Laboratory, British Geological Survey, Nicker Hill, Keyworth, Nottingham, NG12 5GG, United Kingdom

[4]Department of Earth Sciences, Natural History Museum, Cromwell Road, London, SW7 5BD, United Kingdom.

[5]British Geological Survey, Nicker Hill, Keyworth, Nottingham, NG12 5GD, United Kingdom

[6]Currently at: Geological Survey Ireland, Beggars Bush, Haddington Road, Dublin D04 K7X4, Ireland

***Correspondence:** s.l.broom-fendley@ex.ac.uk

Keywords:

Songwe Hill; carbonatite; Chilwa Alkaline Province; REE; U-Pb dating; HREE; apatite

Highlights:

- Songwe Hill is a multi-phase intrusion, emplaced at a shallow depth in the crust
- Evidence for pervasive late (carbo)-hydrothermal overprinting
- Interaction with late fluids led to HREE mineralisation

- A large local heat source differentiates Songwe Hill from the other Chilwa Alkaline Province carbonatites

Abstract

Songwe Hill, Malawi, is one of the least studied carbonatites but has now become particularly important as it hosts a relatively large rare earth deposit. The results of new mapping, petrography, geochemistry and geochronology indicate that the 0.8 km diameter Songwe Hill is distinct from the other Chilwa Alkaline Province carbonatites in that it intruded the side of the much larger (4 x 6 km) and slightly older (134.6 ± 4.4 Ma) Mauze nepheline syenite and then evolved through three different carbonatite compositions (C1–C3). Early C1 carbonatite is scarce and is composed of medium–coarse-grained calcite carbonatite containing zircons with a U–Pb age of 132.9 ± 6.7 Ma. It is similar to magmatic carbonatite in other carbonatite complexes at Chilwa Island and Tundulu in the Chilwa Alkaline Province and others worldwide. The fine-grained calcite carbonatite (C2) is the most abundant stage at Songwe Hill, followed by a more REE- and Sr-rich ferroan calcite carbonatite (C3). Both stages C2 and C3 display evidence of extensive (carbo)-hydrothermal overprinting that has produced apatite enriched in HREE (<2000 ppm Y) and, in C3, synchysite-(Ce). The final stages comprise HREE-rich apatite fluorite veins and Mn-Fe-rich veins. Widespread brecciation and incorporation of fenite into carbonatite, brittle fracturing, rounded clasts and a fenite carapace at the top of the hill indicate a shallow level of emplacement into the crust. This shallow intrusion level acted as a reservoir for multiple stages of carbonatite-derived fluid and HREE-enriched apatite mineralisation as well as LREE-enriched synchysite-(Ce). The close proximity and similar age of the large Mauze nepheline syenite suggests it may have acted as a heat source driving a hydrothermal system that has differentiated Songwe Hill from other Chilwa carbonatites.

1. Introduction

Since the discovery of carbonatites in Africa (Dixey et al., 1937), many of the carbonatite complexes of the Chilwa Alkaline Province of Malawi have been extensively studied and documented, resulting in excellent memoirs on Chilwa Island (Garson and Campbell Smith, 1958), Tundulu (Garson, 1962) and Kangankunde (Garson and Campbell Smith 1965). However, the Songwe Hill carbonatite, which is the fourth largest in the province, was not subject to the same extensive surveying and mapping as the other nearby complexes (e.g. Garson and Walshaw, 1969) and only short summaries exist in the literature (Garson, 1965, 1966; Woolley, 2001; Harmer and Nex, 2016).

Interest in the Songwe Hill carbonatite has largely stemmed from exploration for rare earth elements (REE). Building on earlier descriptions of other occurrences in the area (e.g. Garson, 1962), a brief overview of the Songwe Hill carbonatite and related rocks was first provided by the Nyasaland Geological Survey who indicated the presence of REE minerals (Garson, 1965; Garson and Walshaw 1969). Further exploration for REE was carried out at Songwe Hill between 1986 and 1988 by the Japanese International Co-operation Agency (JICA) and the Metal Mining Agency of Japan (MMAJ). They concluded that Songwe Hill, as well as other occurrences within the Chilwa Alkaline Province, had "*high potentiality for a carbonatite deposit*" (JICA and MMAJ, 1989). Recent work by Mkango Resources has established a (NI 43-101 compliant) probable mineral reserve for the REE of 8.4 million tonnes at 1.6% TREO, with a higher proportion of HREE than many other carbonatite-related REE deposits (TREO = Total Rare Earth Oxides; Croll et al., 2014; Harmer and Nex, 2016). This contribution summarises many of the findings, including geological, mineralogical, geochemical and age data, from this most-recent exploration at Songwe. With these new data, we discuss the evolution of this intrusion in the context of other intrusions in the Chilwa Alkaline Province. Details on the REE mineralogy are presented in a separate contribution (Broom-Fendley et al., 2017).

2. Geological setting

Songwe Hill is located in the Phalombe district of south-eastern Malawi, an area where the regional basement comprises Neoproterozoic gneisses and granulites. These have undergone several stages of intrusion and deformation, including emplacement of a much earlier episode of late Precambrian alkaline magmatism in the north and south of the country (Bloomfield, 1968; 1970; Eby et al., 1998; Kröner et al., 2001; Ashwal et al., 2007). This earlier episode is suggested to be associated with an ancient continental rift zone (Burke et al., 2003). Regional Pan-African deformation is manifested through metamorphic overprinting (e.g. Woolley et al., 1996) and emplacement of granitic intrusions (Haslam et al., 1983). A subsequent Jurassic (Karroo) basic dyke swarm is prevalent throughout the south of the country (Woolley et al., 1979; Macdonald et al., 1983).

Songwe Hill is part of the Late Jurassic–Early Cretaceous Chilwa Alkaline Province: a region approximately 300–400 km in diameter in the south of Malawi and in Mozambique (Fig. 1). The province is made up of an essentially intrusive suite of carbonatite, nephelinite, ijolite, nepheline syenite, syenite, quartz syenite and granite (Woolley and Garson, 1970; Woolley, 1991, 2001).The Chilwa Alkaline Province intrudes the basement in a variety of styles, including large plutons, carbonatite-bearing ring complexes, alkaline dyke swarms following NE/SW lines of crustal weakness, small nephelinite and phonolite plugs and small breccia vents (Woolley, 2001). Volcanic phonolites, nephelinites and blairmorites of the Lupata-Lebombo area in Mozambique are also considered to be associated with the Chilwa Alkaline Province as they are of similar composition and age (Woolley and Garson, 1970). Subsequent to the Chilwa Alkaline Province volcanism, the region has been eroded, possibly deeper in the east than in the west (Eby et al., 1995), such that many of the intrusions are now isolated inselbergs within a Cenozoic lacustrine peneplain.

Songwe Hill forms a steep-sided conical hill, approximately 800 m in diameter, rising about 230 m from the surrounding plain. The hill abuts the north-western flank of Mauze, a large,

oval, nepheline syenite intrusion which is approximately 6×4 km in area and 800 m high. To the north-west and north-east are two, lower-lying, hills: Chenga and Pindani (Figure 2A).

3. Geology of Songwe Hill

Mapping and a two phase diamond drilling campaign, totalling approximately 6850 metres, were conducted by Mkango Resources between 2011 and 2012 (Croll et al., 2014). These activities focussed on the central and northern flanks of Songwe Hill, where most of the known REE mineralisation occurs (Figure 2B). Carbonatite outcrops broadly follow two lobate structures, trending SW-NE, intruding into the fenite host. To simplify the mapping process, however, small-scale heterogeneities such as fenite blocks and minor veins, were excluded. Drilling highlighted that these heterogeneities continue with depth and greatly complicate any structural interpretation. REE mineralisation occurs predominantly in carbonatite, but also in fenite, up to 350 m below the surface of the hill. No clear contact between Songwe and Mauze, or the basement, was encountered during drilling and surface contacts are obscured by cover (Croll et al., 2014).

Samples were collected over two field seasons in 2011 and 2012. Petrography was carried out using similar techniques to those described by Broom-Fendley et al (2016a). Cold cathodoluminescence (CL), using a CITL Mk3a electron source operated at 3–13 kV and ~350 nA, was primarily used for mineral identification, in combination with standard optical petrography. Selected samples were also analysed using BSE imagery and qualitative EDS analyses, using a JEOL JSM-5400LV SEM and a JEOL JXA-8200 electron microprobe, to confirm the identity of some minerals.

The main geological units comprise: variably fenitized basement granulite, gneiss and dolerite dykes; clast supported fenite breccia; fenite; carbonatite; and late-stage veins of apatite- and fluorite-rich rock, and Mn- and Fe-rich rock. New field observations, petrographic and geochemical data are presented for these units in the following sections.

3.1 Clast-supported fenite breccia

The outermost unit at Songwe comprises a clast-supported breccia formed of large angular slabs of country rock gneiss and dolerite. This unit is most prominent on Chenga Hill, north-west of the main Songwe Hill intrusion (Fig. 2A). The exposure of this unit is limited. However, based on comparison with other carbonatites in the Chilwa Alkaline Province, it presumably extends around the edge of the intrusion (c.f. Chilwa Island, Nkalonje, Tundulu; Garson and Smith, 1958, Garson, 1965). This rock is only fenitised to a low degree, with K-feldspar replacement most-prominent at the edges of the gneiss clasts while the centre retains the original mineralogy and banding (Figure 3A). As such, it differs considerably from the majority of fenite at Songwe.

3.2 Fenite

Songwe Hill is predominantly composed of fenite, which forms the entirety of the lower flanks of the hill and extends at least 500 m away from the intrusion, although the full extent is not known as the contact with low-grade fenite breccia is obscured by sediment. Major carbonatite outcrops are restricted to the upper parts of the hill (mapped in Fig. 2B). Within the carbonatite, fenite also occurs as large blocks/boulders (>100 m) down to small, angular, clasts (<1 mm) (Figure 3B). Fenite blocks and clasts are found at the greatest depths sampled in most drill-holes (e.g. 302 m, hole PX001). The large blocks of fenite appear to be in-situ, or transported a very short distance and are interpreted as fractured blocks from the margins, or the roof, of the carbonatite. At the summit of the hill, fenite is continuous with only rare carbonatite veinlets, suggesting that the roof zone of the carbonatite is exposed and, therefore, that the carbonatite never reached the surface.

In many fenite samples a coarse-grained equigranular igneous texture is preserved, strongly suggesting an igneous protolith, highly likely to be nepheline syenite from the neighbouring Mauze intrusion. Other clasts are fine grained and are highly likely to be altered phonolite.

Little evidence of banding, as seen in the country rock around Songwe, occurs in the fenite clasts.

Fenitization is predominantly potassic, and where rocks have been completely fenitized they are composed almost entirely of orthoclase with minor aegirine. Other minor phases include fluorapatite, zircon, rutile, ilmenite and hematite (commonly altered to goethite). In small clasts within the carbonatite, fenite commonly contains a proportion of carbonate, likely to be derived from carbonatite emplacement.

3.3 Carbonatite

Songwe Hill comprises three main stages of carbonatite intrusion: coarse grained calcite carbonatite (sövite); fine-grained calcite carbonatite (alvikite); and Fe-rich ferroan calcite carbonatite. The terms C1–C3 are used as shorthand to distinguish the different carbonatite types (Table 1). While the terminology broadly overlaps with the terminology used by Le Bas (1977, 1987, 1999), it is important to distinguish that the C3 ‘ferrocarbonatite’ is not, in the strict sense, accurate, as the Fe in these rocks is hosted in oxide minerals (Gittins and Harmer, 1997).

3.3.1 Calcite carbonatite (C1 and C2)

Coarse-grained calcite carbonatite (C1) is rare at Songwe and only occurs as rounded clasts, of up to a few cm, in other carbonatite types (Figure 3C). It is composed of medium-grained anhedral calcite (90 vol. %), minor anhedral ankerite (5 vol. %) and an assemblage of ovoid apatite, subhedral zircon, euhedral pyrite, anhedral pyrochlore and anhedral K-feldspar (Figure 4A). Zircon grains are euhedral to subhedral, and range from small (approximately 50 µm; Figure 5A–B) to relatively large grains (up to 0.5 mm), the latter of which can exhibit well developed zoning (Figure 5D–E). Based on their habit, formation at calcite grain boundaries and association with ovoid apatite, zircons in coarse-grained carbonatite are interpreted as a carbonatite magmatic phase.

Fine grained calcite carbonatite (C2) is the most abundant carbonatite type at Songwe, and the term includes all fine-grained white–grey calcite carbonatites. It ranges from calcite-rich rocks through to complex, multi-phase samples but most commonly comprises fine-grained calcite with minor interstitial ankerite (Figure 4B). Anhedral apatite stringers cross-cut earlier calcite (e.g. Figure 4B). Calcite in association with these apatite-stringers luminesces brighter in CL images than earlier-crystallising calcite, associated with increasing Mn relative to Fe. In some samples xenocrysts of zircon, pyrochlore, pyrite and K-feldspar are present and are rounded and altered to varying degrees. Pyrite, zircon and K-feldspar show little rounding and are found in bands while pyrochlore is commonly rounded and partially fractured. Zircons in the fine-grained calcite carbonatite are small, subhedral and appear out of equilibrium with the host rock, as indicated by edges that are embayed and cores that are pitted and corroded (Figure 5C). Localised assemblages of euhedral synchysite-(Ce), baryte, and anhedral strontianite are disseminated throughout the carbonatite (Figure 4C).

3.3.2 Ferroan calcite carbonatite (C3)

Ferroan calcite carbonatite (C3) is fine-grained and occurs as veins in calcite carbonatite, as breccia clasts and as large discreet masses. It is found throughout the intrusion but is most abundant towards the centre (Figure 2B). It commonly contains clasts of fenite and, less commonly, clasts of both coarse- (C1) and fine-grained calcite carbonatite (C2). It weathers dark brown–black and on a fresh surface it is dark, fine-grained and commonly banded (Figure 3D). The bands include (A) a ferroan calcite carbonatite groundmass, (B) pale apatite-bearing layers and (C) similarly pale LREE-fluorcarbonate-bearing layers.

The (A) ferroan calcite carbonatite groundmass is predominantly (95 vol. %) composed of an opaque carbonate which luminesces dark orange in CL images. This phase is likely to be an altered Fe-bearing calcite which has exsolved Fe from its structure. Minor hematite (4 vol. %) and zircon (1 vol. %) are also present in the groundmass. Zircon is subhedral and shows resorption textures indicating that it is out of equilibrium with the host rock. Apatite bands (B)

are monomineralic. The apatite is anhedral, very fine-grained and forms mm–cm bands, similar to those in fine-grained calcite carbonatite (Figure 4B). They are commonly aligned with each other and with the later LREE-fluorcarbonate-bearing assemblage (C). This assemblage is similar to the LREE-bearing assemblage found in vugs in the C2 calcite carbonate, and is composed of syntaxial intergrowths of euhedral synchysite-(Ce) and parisite-(Ce), euhedral baryte and anhedral strontianite or calcite (Figure 4D). Cross-cutting relationships between the various stages are evident from the termination of an apatite stringer by a REE-fluorcarbonate-bearing assemblage (Figure 4D), and from the presence of partially fragmented apatite in a matrix of strontianite and fluorcarbonates (Figure 4E).

3.4 Late-stage veins

Throughout the carbonatite several stages of overprinting and late cross-cutting veins are evident. These are subdivided into fluorite/apatite–fluorite enriched rocks and Mn-Fe-veins.

3.4.1 Apatite-fluorite veins

Small veins, rich in fluorite and apatite, form a volumetrically minor part of the carbonatite and are most conspicuous in the breccia at Chenga Hill (Figure 3A). Similar fluorite-rich areas are also found in drill core, most prominently in core PX0016 (Croll et al., 2014). In addition, early descriptions of Songwe Hill identified similar apatite-fluorite rock in boulders approximately half a mile north-east of Songwe (Garson, 1965). In previous contributions (e.g. Broom-Fendley et al., 2016b) these veins have been termed ‘C4’. However, this term has been discontinued as it suggests the veins are a variety of carbonatite.

The apatite-fluorite veins comprise major fluorite, apatite, calcite/ferroan-calcite, quartz and baryte (Figure 4F). Accessories include xenotime, zircon, rutile/anatase, Mn-oxides, hematite, and synchysite/parisite. Fluorite is sub–anhedral and typically occurs in elongate stringers and in discrete patches. Individual grains vary in size from 20–200 μm, with most typically around 20–50 μm. Apatite is subhedral and typically clumps together in veins

formed of equigranular crystals approximately 150–200 µm in size. Fragments of broken K-feldspar are common in the apatite-fluorite rock. The pieces are angular and show little evidence of alteration or reaction. Late-stage minerals include anhedral baryte and quartz.

3.4.2 Mn-Fe-veins

Mn-Fe-rich rocks form along centimetre to metre wide veins, following straight fractures cross-cutting carbonatite and fenite (Figure 3B). These are especially common at the edge, and towards the top, of the intrusion, cutting the fenite roof-zone. The rocks are composed of a mixture of carbonate rhombs and Fe- and Mn-oxides, commonly altered to limonite. In thin-section they exhibit distinct alteration halos, where Fe-bearing carbonates in the carbonatite are decomposed and replaced by Fe-oxides.

Mn-Fe-rocks can occur as areas of large-scale alteration and in these circumstances the relation with the host-rock is difficult to establish. These areas are deeply weathered and revealed by bulldozed road-cuts or as pockets at depth in drill core (Figure 3F). These rocks are typically carbonate-poor compared to their vein-hosted counterparts, and are predominantly composed of massive Mn- and Fe-oxides, with little evidence of other minerals.

4. Whole-rock Geochemistry

Whole-rock analyses were carried out on core samples (marked on Fig. 2B), drilled by Mkango Resources Ltd in 2011. Samples were taken between 0.3 and 1 m intervals, at the point of lithological change. Rock powders were analysed for major elements by ICP-OES and trace elements by ICP-MS at Intertek-Genalysis in Australia using technique FP6/MS33 (Intertek-Genalysis internal catalogue number, see www.genalysis.com.au/minerals/assay). This technique involves digestion using a sodium peroxide fusion to dissolve refractory minerals. Unfortunately, however, this means no Na data are available for the whole-rock analyses. Fusion products are dissolved in HCl and diluted for analysis and the results are

corrected for dilution and the amount of flux used for digestion. Internal standards were used to correct for drift, viscosity effects and plasma fluctuations. Repeat blind analyses of commercial carbonatite reference standards AMIS0185 (n = 91) and GRE-04 (n = 105) indicate no significant departures from published major and trace element concentrations, with 2σ values generally lower than the quoted uncertainty in the reference material (Supplementary Table 1). Owing to the fine-grained and heterogeneous nature of the samples, some carbonatite analyses incorporate a significant proportion of Al_2O_3, SiO_2, and K_2O derived from fenite (Supplementary Figure 1). Therefore, carbonatite analyses with >2 wt. % Al_2O_3 are considered contaminated with fenite and are excluded from interpretation.

A summary of major and trace element whole-rock data is presented in Table 2 (full dataset Supplementary Table 2). Regardless of the absence of Na_2O values from the whole-rock analyses (owing to preparation with a Na-peroxide fusion), most of the fenite analyses give totals close to 100%, reflecting the K-feldspar-rich nature of these samples. Carbonatite contamination in these analyses is indicated by elevated average loss on ignition (LOI) values (15.5 Wt. %) and the correlation of LOI with SrO, MgO, CaO, and the REE. Given the dominant role of even small amounts of carbonatite for the REE concentration, the REE content of ‘pure’ fenite is undoubtedly very low.

Carbonatite analyses are split between calcite carbonatite (C2) and ferroan-calcite carbonatite (C3) (Table 2). The small clast size and scarcity of material from the coarse-grained C1 calcite carbonatite means that no data are available for this rock type. With the exception of P_2O_5, SrO, Th and REE, average concentrations for most elements are similar for both C2 and C3 carbonatite (Table 2). Using either of the ternary carbonatite classification diagrams (IUGS classification of Wt. % oxide [Woolley and Kempe, 1989; Le Maître, 2002] or molar proportions [Gittins and Harmer, 1997]), calcite carbonatite plots between the calciocarbonatite and ferruginous calciocarbonatite fields while ferroan calcite carbonatite forms a small cluster, broadly within the ferruginous calciocarbonatite field

(Figure 6). Despite the assignation of C3 as a Fe-rich carbonatite, it should be stressed that the dominant mineralogical control on the Fe concentration is not a Fe carbonate, but rather Fe oxides or hydroxides. This is best evaluated on a plot of LOI against total MnO+FeO (Figure 7A), where LOI is assumed to be directly proportional to CO_2 concentration. There is a significant decrease in LOI with increasing FeO content for C2 and C3 carbonatites corresponding with mixing lines between Fe oxide minerals and calcite. While pyrite occurs as a minor mineral in these rocks, it is not abundant enough to account for the large variations in Fe content. A large contribution from siderite can also be excluded as this would result in a high FeO concentration whilst retaining a high LOI, a trend not shown in the data (Figure 7A). However, a minor amount of ankerite in the rocks is likely as indicated by the correlation between MgO and FeO (Figure 7B). This contribution from ankerite is highly likely to account for the scatter in LOI and Fe contents for C2 and C3 data (Figure 7A). The carbonatite analyses show a positive trend between MnO+FeO with SrO and REE (Figure 7C–D), a common feature of more Fe-rich carbonatites and accounted for by the crystallisation of strontianite and REE fluorcarbonates in these samples (Le Bas, 1989).

Mn-Fe-veins have much higher average FeO and MnO concentrations and lower MgO, SrO and LOI values than both analysed carbonatite types (Table 2, Figure 7A–C). On a ternary plot (Figure 6), these rocks form a continuum between calcite carbonatite and ferrocarbonatite, as would be the case for mixtures of calcite and Fe-/Mn-oxides. Mixing is also supported by the trends in Figure 7A, where the Mn-Fe-vein data plot between carbonatite compositions and a hematite/goethite endmember, suggesting these samples are the result of carbonate removal and, therefore, residually enriched in Fe oxides. Mn-Fe-veins do not show any relationship between REE, SrO and MnO+FeO contents and have similar REE concentrations to both C2 and C3 carbonatites.

REE concentrations in the Songwe carbonatites range from approximately 5000–60,000 ppm, with ferroan calcite carbonatite typically more REE-rich, averaging between 25,000 and

60,000 ppm (Figure 7C). All rock types at Songwe are LREE enriched (Figure 8A), a feature common to most carbonatites (e.g. Jones et al., 2013). The degree of LREE enrichment increases in later C3 carbonatites and, to a lesser extent, in the Mn-Fe-veins (Figure 8B). However, in the latest apatite-fluorite rocks, LREE contents are similar to those of C2 carbonatite, while the HREE contents are relatively enriched. In these rocks, Y concentrations average 1135 ppm, approximately double the average for carbonatites at Songwe Hill, while having similar total REE contents. The elevated HREE contents correspond to higher P_2O_5 concentrations, reaching >1500 ppm Y and >10.72 Wt. % P_2O_5 (Figure 7F), and indicate that apatite is hosting the HREE at Songwe, as it is the most abundant phosphate mineral present (Broom-Fendley et al., 2017).

5. U–Pb age determinations

5.1 Analytical and data processing procedures

Geochronological data from zircons in C1 and C2 carbonatites, as well as a sample from the Mauze nepheline syenite, were acquired over three sessions at NIGL (NERC Isotope Geosciences Laboratories). The methodology followed that described in Thomas et al (2010) with data reduction and reporting procedures following those described in Horstwood et al (2016).

While there is a significant fenite contribution to the carbonatite at Songwe, it is highly likely the zircons from C1 carbonatite crystallised from a carbonatite melt, rather than entrained as xenocrysts from the surrounding rocks. This is demonstrated by their formation at carbonate grain boundaries and association with rounded apatite grains, indicating crystallisation prior to carbonate (Figure 4A). Furthermore, the majority of these grains are relatively small (~0.2 mm) and exhibit little zoning (e.g. Figure 5A–C). Comparing the carbonatite zircons with those from fenite and nepheline syenite (the two most-proximal potential contamination sources) with those from carbonatite indicates that the carbonatite zircons are texturally

distinct, exhibiting different luminescence colours crystal habit and zoning (Supplementary Figure 2).

The zircons were ablated in-situ using a New Wave Research UP193SS (193 nm), Nd:YAG laser ablation system fitted with a Large Format Cell (holding 6 standard-sized polished thin sections) coupled to a Nu Instruments Nu Plasma HR MC-ICP-MS. Operational parameters for laser ablation and mass spectrometry are detailed in Supplementary Table 3 with further methodology details in the Supplementary Information.

Data were normalised using '91500' as the primary zircon reference material with 'Mud Tank' and 'GJ1' used as validation materials to determine accuracy and the long-term uncertainty for propagation. The U and Pb concentration of all zircon analyses was generally low, averaging ca. 2 ppm Pb and ca. 100 ppm U with many analyses well below this. Combined with the required spatial constraints based on CL imaging, this necessitated using a 35 µm ablation spot size. At these low concentrations Mud Tank represents a useful validation material (ca. 2 ppm Pb, 20 ppm U), capturing the long term excess variance uncertainty component (2.1% 2σ U–Pb) not reflected when analysing higher U reference materials such as GJ1 (no excess variance in U–Pb over the study, see Supplementary Table 4). Propagating this systematic, long-term excess variance uncertainty into the weighted mean uncertainty of the sample result, follows community-derived guidelines recommended in Horstwood et al (2016), and accounts for systematic shifts between sessions for results from low U materials. This demonstrates that the results from the different sessions for these low U materials are within uncertainty of each other (N.B. the higher U concentration GJ1 did not show such session biases). U–Pb dates for each session, with and without propagation for their systematic uncertainty component, are listed in Table 3. Final ages are quantified as the average from all sessions ± the maximum range of session results allowing for the propagated session uncertainties. This uncertainty range equates to 3.8–6.7 Ma on the average and therefore encompasses the systematic uncertainty level (typically 3–4 Ma 2σ). Using reference values from Horstwood et al (2016), validation results from all sessions for

Mud Tank and GJ1 (without propagation for systematic uncertainties) demonstrate accurate results within the defined uncertainties (i.e. bias < uncertainty) with those data for Mud Tank highlighting the need for an additional variance component ($^{206}Pb/^{238}U$ = 0.11996 ± 0.48%, MSWD = 4.3, n= 27, Bias = -0.21%, long term variance = 2.1% 2σ; see Supplementary Table 4 and Supplementary Figure 3).

5.2 *Results*

All data reflect the presence of small amounts of common-Pb however ^{204}Pb is not resolvable by the LA-ICP-MS method used. As such, sample ages are interpreted using Tera-Wasserburg plots (e.g. Fig 9). Zircons from two calcite carbonatite (C1) samples (T0218 & T0206) were analysed in three different sessions over a period of 3 months returning ages between 129.5 ± 3.3/4.3 and 137.3 ± 1.0/3.1 (2σ, MSWD = 1.8, n=11), with both within-session and between-session uncertainties quoted following Horstwood et al (2016). The results are equivalent allowing for their systematic uncertainties and are combined in an average and maximum range of 132.9 ± 6.7 Ma. Zircons from a single C2 calcite carbonatite were dated in one session only, defining an age of 135.6 ± 2.5/3.8 (2σ, MSWD = 1.9, n=5) after systematic uncertainty propagation.

Zircons from Mauze (sample U4913) were analysed in two different sessions 3 months apart, returning ages between 137.5 ± 1.5/3.3 Ma (2σ, MSWD = 3.6, n=18) and 131.7 ± 0.9/2.9 Ma (2σ, MSWD = 6.1, n=43). The results are within uncertainty after propagation and are combined in an average and maximum range of 134.6 ± 4.4 Ma. As such, it is indistinguishable in age isotopically from the Songwe samples even though field relationships indicate that it is older (see below).

6. Discussion

6.1 Order of emplacement and fluid evolution

Field relationships indicate that the Songwe carbonatite intruded and fenitised the Mauze nepheline syenite and is, therefore, younger. The principal evidence for this is the equigranular texture of the fenite, incorporating large rectangular pseudomorphs of feldspar which is texturally reminiscent of the neighbouring nepheline syenite. Blocks of this material have been veined, brecciated and incorporated into the intruding carbonatite. These field relationships provide a better constraint on the relative age of the intrusion events than the radiometric ages of Songwe (132.9 ± 6.7 Ma) and Mauze (134.6 ± 4.4 Ma).

Carbonatites are theorised as being generated via one of two principal mechanisms: (1) as 'segregations' from a carbonated silicate melt, either through (a) liquid immiscibility (Kjarsgaard and Hamilton, 1989; Lee and Wyllie 1997, 1998) or (b) as a residual melt fraction after silicate fractionation (Gittins, 1989; Lee and Wyllie, 1994). Alternatively (2), they could be generated from melting CO_2-bearing peridotite directly from the mantle (Wallace and Green, 1988; Harmer and Gittins, 1998; Brey et al., 2008). Gittins and Harmer (2003) argue that even where silicate rocks accompany carbonatites, the two may not be genetically related, favouring a model where two separate melts utilise the same conduits to reach the crust from the mantle. Owing to the lack of analyses from the Mauze intrusion, there is insufficient geochemical data to robustly comment on the relationship between the Songwe carbonatite and Mauze nepheline syenite. However, the indistinguishable emplacement ages of the two intrusions provides circumstantial evidence of a genetic connection, suggesting direct emplacement of carbonatite from the mantle may not be an appropriate model (cf. Xu et al., 2015).

A common compositional trend during the evolution of many silicate-poor carbonatites is from calcium-rich to magnesium- and iron-rich compositions with decreasing P, Zr, Nb and

400 increasing LREE and F (e.g. Le Bas, 1987, 1989; Hamilton et al., 1989; Thompson et al.,
401 2002). These trends represent a 'typical' evolution path for a Si-depleted carbonatite,
402 dominated by fractional crystallisation of carbonates, as well as apatite and pyrochlore (Le
403 Bas, 1989; Kjarsgaard and Hamilton, 1989; Hamilton et al., 1989). For instance, Xu et al.,
404 (2010) showed that continued fractionation of carbonates at the Miaoya carbonatite, China,
405 can lead to progressive enrichment in the light REE. This common chemical evolution is
406 reflected by the carbonatite compositions at Songwe where Fe-rich carbonatites (C3) are
407 more enriched in LREE and SrO than C2 calcite carbonatite (Figure 7C). C1 carbonatites,
408 comprising relatively coarse-grained apatite, zircon and calcite, might, by analogy with more
409 deeply eroded carbonatites (e.g. Le Bas, 1977, 1987), represent a cumulate developed from
410 a lower level of the intrusion. Their presence at depth is evidenced by the occurrence of
411 coarse calcite carbonatite clasts in the later carbonatite varieties (Figure 3E).

412 During the later stages of emplacement, carbonatites transition from a magmatic to a
413 hydrothermal regime and fluids are expelled (Rankin, 2005). These fluids commonly lead to
414 LREE, barite, strontianite and fluorite mineralisation, manifested in veins, or disseminated
415 throughout the host carbonatite (e.g. Mariano, 1989; Ngwenya, 1994; Wall and Mariano,
416 1996; Andrade et al., 1999; Wall and Zaitsev, 2004; Doroshkevich et al., 2009; Nadeau et
417 al., 2015). Several features, such as crystallisation of LREE minerals in veins and in small
418 cavities, were identified by Broom-Fendley et al., (2017) who ascribe a similar role for a
419 hydrothermal component to the LREE mineralisation at Songwe.

420 **6.2 (Carbo)-hydrothermal alteration**

421 Despite the 'typical' evolution of the carbonatite at Songwe towards more Fe- and REE-rich
422 compositions, some notable exceptions are apparent. One such example is the correlation
423 between P_2O_5 and the HREE (Fig. 7F), which has not been previously documented in
424 carbonatites. Correlation between P_2O_5 and the HREE is controlled by the uptake of the
425 HREE in late-stage apatite at Songwe (Broom-Fendley et al., 2017). Late apatite forms

anhedral stringers and cross cuts many carbonate phases (Broom-Fendley et al., 2017; Figs 4D–E). Late apatite is apparent in all carbonatite types at Songwe, and is independent of SrO, LREE and FeO contents. The disconnect between these common indicators of carbonatite evolution from the P_2O_5 and HREE contents suggests HREE-enrichment and P_2O_5-bearing mineral crystallisation is an artefact of a late-stage fluid at Songwe, cross-cutting the principal carbonatite types. The products of such a fluid are locally manifested as apatite-fluorite-veins, which have notably higher HREE contents than the other carbonatite units at Songwe (Fig. 8B).

Further evidence for a hydrothermal contribution to the evolution of Songwe is indicated by the presence of a Y/Ho anomaly in the whole-rock REE distribution of all the carbonatite types (Fig. 8). While the magnitude of this Y/Ho anomaly is quite small, repeat analyses of the AMIS0185 and GRE-04 carbonatite standards indicate the data are accurate and the Y anomaly is related to natural processes and the anomaly is, therefore, significant to carbonatite evolution (Supplementary Table 1). This process is likely to be a hydrothermal overprint as fractionation of Y is generally considered to be caused by the preferential transport of Y, over the other HREE, in F-bearing aqueous fluids (Bau and Dulski, 1995; Bau, 1996; Loges et al., 2013). Regardless of the likelihood that the fluid is H_2O-rich, a significant carbonate component cannot be discounted and the late fluids at Songwe are therefore termed (carbo)-hydrothermal. The presence of the Y/Ho anomaly throughout all analysed carbonatite types indicates these (carbo)-hydrothermal fluids overprinted all of the carbonatites (C1–C3; Bühn, 2008; Broom-Fendley et al., 2017).

Cross-cutting relationships indicate that Mn-Fe veins are the last stage to occur at Songwe, predominantly following brittle fractures. Mn-Fe-veins are composed of oxide minerals which are likely to be the result of the de-carbonation of previous carbonatites. This genesis is supported by the erratic composition of the Mn-Fe-veins, which contain a variable CaO and FeO content suggestive of partial $CaCO_3$ dissolution (Fig. 6). This is also supported by

petrographic observations, where samples from the centre of a vein are more calcite-poor than those from the edge of a vein. Low SrO and MgO concentrations in these rocks, compared with C2 and C3 carbonatites, indicates these elements have been removed during dissolution. Similar rock types to the Mn-Fe-veins have been described from other locations, summarised as hematite carbonatites by Andersen (1987a, b). Examples include: Fen, Norway; Lueshe, DR-Congo; and several locations in Kenya (Andersen, 1984, 1987b). These rocks are interpreted as the products of post-magmatic dissolution of Fe-rich carbonatite under oxidising conditions, where Fe is immobile (Andersen, 1987b). Based on O isotope analyses, Andersen (1987a) interprets the alteration to have been caused by meteoric water, after the last stages of intrusion.

6.3 A shallow carbonatite

While a hydrothermal component is generally required to generate ore grades of LREE, extensive remobilisation of the HREE is much less common. Extensive hydrothermal overprinting of the HREE does not occur in other carbonatites of the Chilwa Alkaline Province, suggesting Songwe is unique in some aspect. One such aspect could be the mineralising fluid source. Stable (C and O) data for apatite and calcite at Songwe indicate a likely meteoric contribution to the apatite mineralisation and, potentially, to calcite crystallisation. However, a contribution from magma degassing and carbonatite-derived fluid cannot be entirely discounted (Broom-Fendley et al., 2016b). A contribution from meteoric water suggests a shallow intrusion level and is consistent with the strong evidence from the abundance of fenite and lack of carbonatite at the top of the hill, probably indicating that the carbonatite has not intruded above the current erosion depth. A shallow intrusion level is also supported by the presence of brittle deformation, occurring both in fenite around the carbonatite (e.g. Figure 3A) and in breccia clasts and stoped blocks within the carbonatite. Such extensive brecciation indicates a change from lithostatic to hydrostatic pressure, which occurs at shallow crustal levels. This local field evidence is also supported by apatite fission-

track ages from other intrusions in the Chilwa Province. These ages indicate the other intrusions cooled rapidly and were therefore emplaced at a shallow level (Eby et al., 1995).

Given the features discussed above, we suggest that Songwe Hill, at its current level of erosion, is the highest level of a shallow, subvolcanic magma chamber. It is likely that a 'head' of volatiles or late magmatic pulses has successively pooled in these upper levels, interacting with meteoric water, and resulting in multiple stages of hydrothermal overprinting and mineralisation. Rounded clasts of the carbonate-rich breccias and pervasive hydrothermal overprinting suggests widespread degassing and volatile loss from a carbonatite magma.

6.4 Comparison with other Chilwa intrusions

The new U-Pb zircon ages indicate that Songwe is a similar age to the other major carbonatite complexes in the Chilwa Alkaline Province (Figure 1). Indeed, many parallels can be drawn between Songwe and these other large Chilwa carbonatite complexes. Carbonatites at Tundulu and Chilwa Island progressively evolve to increasing Fe and REE concentrations (Garson and Smith, 1958; Garson, 1962) while there is evidence for late HREE-enrichment in apatite at Tundulu and in minor rocks at Kangankunde (Broom-Fendley et al., 2016a). Furthermore, brecciation of country rock around these intrusions is common, with contact breccias and fenite breccia occurring at all localities. Cooling rates for other intrusions in the Chilwa Alkaline Province also suggest a shallow intrusion level (Eby et al., 1995). However, there are also significant differences between Songwe and other Chilwa Alkaline Province carbonatites. Whereas some carbonatites in the province are geographically, and in some cases temporally, accompanied by silicate rocks, the volume of silicate rock exposed is much lower, relative to the volume of nepheline syenite at Mauze adjacent to Songwe. This difference could be important in differentiating the HREE occurrences at Songwe Hill from the other intrusions of the Chilwa Alkaline Province. Given that the U–Pb age of Mauze is within the uncertainty of the age of Songwe, it is likely that

Mauze was still hot when Songwe intruded. Hydrothermal activity, with temperatures calculated by Ti in zircon thermometry of approximately 500–600°C, was estimated to continue at Zomba (another Chilwa intrusion, larger than Mauze; Fig. 1) for up to 3 Ma subsequent to emplacement (Soman et al., 2010). Furthermore, for the same intrusion, Eby et al. (1995) calculated, from K-Ar amphibole and fission-track zircon ages, that the cooling rate of Zomba was approximately 23°C/Ma. These characteristics suggest that, although Mauze is volumetrically less substantial, it could provide a source of sustained heat for many years after emplacement. Such a heat source would drive continued interaction with surrounding groundwater during the emplacement of Songwe. This, in turn, could explain the presence of extensive (carbo)-hydrothermal overprinting and HREE mineralisation at Songwe, which is essentially absent from other Chilwa carbonatites.

7. Conclusions

In this contribution we have summarised the age, geology and geochemistry of the Songwe Hill carbonatite. The earliest carbonatite type (C1) calcite carbonatite (132.9 ± 6.7 Ma) intruded the older Mauze nepheline syenite (134.6 ± 4.4), although the overlapping uncertainty between the absolute ages indicates these intrusions occurred over a short timeframe. The carbonatite evolved through increasingly Fe-rich contents, with an associated increase in REE and Sr, typical of many carbonatites. However, Songwe differs from other carbonatites, exhibiting a strong relationship between the HREE and P_2O_5, with apatite as the main HREE host. Cross-cutting relationships and anomalous Y/Ho ratios in all carbonatite types indicates that the HREE mineralisation was caused by the influx of a (carbo)-hydrothermal fluid, potentially sourced from interaction with surrounding groundwater. A high degree of brecciation and a large, contemporaneous, neighbouring heat source (Mauze nepheline syenite) contributed to the extensive development of groundwater circulation which differentiates Songwe from other Chilwa carbonatites in which HREE enrichment is absent or only minor.

Acknowledgements

Thanks are due to A. Lemon, A. Zabula, C. Mcheka, I. Nkukumila (Mkango Resources Ltd.), É. Deady (BGS) and P. Armitage (Paul Armitage Consulting Ltd.) for logistical support and enthusiastic discussions in the field. This contribution benefitted from reviews by Jindřich Kynický and Ray Macdonald, as well as anonymous reviewers, who we thank for their time and insightful comments. This work was funded by a NERC BGS studentship to SBF (NEE/J50318/1; S208), the NERC SoS RARE consortium (NE/M011429/1) and by Mkango Resources Ltd. AGG publishes with the permission of the Executive Director of the British Geological Survey (NERC).

References

Andersen, T., 1984. Secondary processes in carbonatites: petrology of 'Rødberg' (hematite-calcite-dolomite carbonatite) in the Fen central complex, Telemark (South Norway). Lithos 17, 227–245

Andersen, T., 1987a. Mantle and crustal components in a carbonatite complex, and the evolution of carbonatite magma: REE and isotopic evidence from the Fen complex, southeast Norway. Chemical Geology 65, 147–166

Andersen, T., 1987b. A model for the evolution of hematite carbonatite, based on whole-rock major and trace element data from the Fen complex, southeast Norway. Applied Geochemistry 2, 163–180

Andrade, F., Möller, P., Lüders, V., Dulski, P., Gilg, H. 1999. Hydrothermal rare earth elements mineralization in the Barra do Itapirapuã carbonatite, southern Brazil: behaviour of selected trace elements and stable isotopes (C, O). Chemical Geology 155:91–113.

552 Ashwal, L., Armstrong, R., Roberts, R., Schmitz, M., Corfu, F., Hetherington, C.,
553 Burke, K., Gerber, M., 2007. Geochronology of zircon megacrysts from nepheline-bearing
554 gneisses as constraints on tectonic setting: implications for resetting of the U–Pb and Lu–Hf
555 isotopic systems. Contributions to Mineralogy and Petrology 153, 389–403

556 Bloomfield, K., 1968. The pre-Karroo geology of Malawi. Memoirs of the Geological
557 Survey of Malawi, 4

558 Bloomfield, K., 1970. Orogenic and post-orogenic plutonism in Malawi. In G. I.
559 Clifford, T.N. (ed.), African Magmatism and Tectonics. Edinburgh, Oliver and Boyd

560 Bau, M. 1996. Controls on the fractionation of isovalent trace elements in magmatic
561 and aqueous systems: evidence from Y/Ho, Zr/Hf, and lanthanide tetrad effect. Contributions
562 to Mineralogy and Petrology 123, 323–333

563 Bau, M. and Dulski, P. 1995. Comparative study of yttrium and rare-earth element
564 behaviours in fluorine-rich hydrothermal fluids. Contributions to Mineralogy and Petrology
565 119, 213–223

566 Brey G.P., Bulatov, V.K., Girnis, A.V., Lahaye, Y., 2008. Experimental Melting of
567 Carbonated Peridotite at 6–10 GPa. Journal of Petrology 49, 797–821

568 Broom-Fendley, S., Styles, M.T., Appleton, J.D., Gunn, G., Wall, F. 2016a. Evidence
569 for dissolution-reprecipitation of apatite and preferential LREE mobility in carbonatite-derived
570 late-stage hydrothermal processes. American Mineralogist, 101, 596–611

571 Broom-Fendley S., Heaton, T., Wall, F., Gunn, G. 2016b. Tracing the fluid source of
572 heavy REE mineralisation in carbonatites using a novel method of oxygen-isotope analysis
573 in apatite: The example of Songwe Hill, Malawi. Chemical Geology, 440, 275–287

574 Broom-Fendley, S., Brady, A.E., Wall, F., Gunn, G., Dawes, W. 2017. REE minerals
575 at the Songwe Hill carbonatite, Malawi: HREE-enrichment in late-stage apatite. Ore Geology
576 Reviews, 81, 23–41

577 Bühn, B., 2008. The role of the volatile phase for REE and Y fractionation in low-
578 silica carbonate magmas: implications from natural carbonatites, Namibia. Mineralogy and
579 Petrology 92, 453–470

580 Burke, K., Ashwal, L., Webb, S., 2003. New way to map old sutures using deformed
581 alkaline rocks and carbonatites. Geology 31, 391–394

582 Croll, R., Swinden, S., Hall, M., Brown, C., Beer, G., Scheepers, J., Redellinghuys,
583 T., Wild , G., Trusler, G., 2014. Mkango Resources Limited., Songwe REE project, Malawi:
584 NI 43-101 pre-feasibility report. Technical report, MSA Group (Pty) Ltd.

585 Dixey, F., Bisset, C., Smith, W., 1955. The Chilwa Series of Southern Nyasaland: A
586 group of alkaline and other intrusive and extrusive rocks and associated limestones. Bulletin
587 of the Geological Survey of Malawi, 5

588 Doroshkevich, A. G., Viladkar, S. G., Ripp, G. S., Burtseva, M. V. 2009.
589 Hydrothermal REE mineralization in the Amba Dongar carbonatite complex, Gujarat, India.
590 The Canadian Mineralogist 47:1105–1116.

591 Eby, G.N., Roden-Tice, M., Krueger , H., Ewing, W., Faxon, E., Woolley, A., 1995.
592 Geochronology and cooling history of the northern part of the Chilwa Alkaline Province,
593 Malawi. Journal of African Earth Sciences 20, 275–288

594 Eby G.N., Woolley, A.R., Din, V., Platt, G., 1998. Geochemistry and petrogenesis of
595 nepheline syenites: Kasungu–Chipala, Ilomba, and Ulindi nepheline syenite Intrusions, North
596 Nyasa Alkaline Province, Malawi. Journal of Petrology 39, 1405–1424

Garson, M.S., 1962. The Tundulu carbonatite ring-complex in southern Nyasaland. Memoirs of the Geological Survey of Malawi, 2

Garson, M.S., 1965. Carbonatites in southern Malawi. Bulletin of the Geological Survey of Malawi, 15.

Garson M.S., 1966. Carbonatites in Malawi. In Tuttle O.F. and Gittins J. (eds) Carbonatites. Interscience Wiley, London.

Garson, M.S., Campbell Smith, W., 1958. Chilwa Island. Memoirs of the Geological Survey of Malawi, 1

Garson, M.S., Campbell Smith, W., 1965. Carbonatite and agglomeratic vents in the western Shire Valley. Memoirs of the Geological Survey of Malawi, 3

Garson, M.S., Walshaw, R., 1969. The geology of the Mlanje area. Bulletin of the Geological Survey of Malawi, 21

Gittins, J., Harmer, R., 1997. What is ferrocarbonatite? A revised classification. Journal of African Earth Sciences 25, 159–168

Gittins, J, Harmer, R.E., 2003. Myth and reality in the carbonatite-silicate rock "association". Periodico di Mineralogia 72, 19–26

Hamilton, D.L., Bedson, P., Esson, J., (1989). The behaviour of trace elements in the evolution of carbonatites. In K. Bell (ed.), Carbonatites: genesis and evolution. Unwin Hyman, London, p.p. 405–427

Haslam H.W., Brewer, M.S., Darbyshire, D.P.F., Davis, A.E., 1983, Irumide and post-Mozambiquian plutonism in Malawi. Geological Magazine 120, 21–35

618 Harmer, R.E., Gittins, J., 1998. The Case for Primary, Mantle-derived Carbonatite
619 Magma. Journal of Petrology, 39, 1895–1903

620 Harmer, R.E., Nex, P.A.M., 2016. Rare earth deposits of Africa. Episodes, 39, 381–
621 406

622 Horstwood, M.S.A., Košler, J., Gehrels, G., Jackson, S.E., McLean, N.M., Paton, C.,
623 Pearson, N.J., Sircombe, K., Sylvester, P., Vermeesch, P., Bowring, J.F., Condon, D.J., and
624 Schoene, B. 2016. Community-derived standards for LA-ICP-MS U-Th-Pb geochronology –
625 uncertainty propagation, age interpretation and data reporting. Geostandards and
626 Geoanalytical Research. Accepted. DOI: 10.1111/j.1751-908X.2016.00379.x

627 Japan International Cooperation Agency, Metal Mining Agency of Japan, 1989.
628 Report on the cooperative mineral exploration in the Chilwa Alkaline Area Republic of
629 Malawi, consolidated report.

630 Jones, A. P., Genge, M., Carmody, L. 2013. Carbonate melts and carbonatites.
631 Reviews in Mineralogy and Geochemistry 75, 289–322

632 Kröner, A., Willner, A., Hegner, E., Jaeckel, P., Nemchin, A., 2001. Single zircon
633 ages, PT evolution and Nd isotopic systematics of high-grade gneisses in southern Malawi
634 and their bearing on the evolution of the Mozambique belt in southeastern Africa.
635 Precambrian Research 109, 257–291

636 Kjarsgaard, B.A., Hamilton, D.L., (1989). The genesis of carbonatites by immiscibility.
637 In K. Bell (ed.), Carbonatites: genesis and evolution. Unwin Hyman, London, p.p. 388–404

638 Le Bas, M.J., 1977. Carbonatite-nephelinite volcanism. John Wiley and Sons Ltd,
639 London

640 Le Bas, M.J., 1981. Carbonatite magmas. Mineralogical Magazine 44, 133–140

641 Le Bas, M.J., 1987. Nephelinites and carbonatites. Geological Society, London,
642 Special Publications 30, 53–83

643 Le Bas, M.J., 1989. Diversification of carbonatite. In K. Bell (ed.), Carbonatites:
644 genesis and evolution. Unwin Hyman, London, p.p. 428–447

645 Le Bas, M.J., 1999. Sovite and alvikite; two chemically distinct calciocarbonatites C1
646 and C2. South African Journal of Geology 102, 109–121

647 Le Bas, M.J., 2008. Fenites associated with carbonatites. The Canadian Mineralogist
648 46, 915–932

649 Le Maitre, R., 2002. Igneous rocks: a classification and glossary of terms:
650 recommendations of the International Union of Geological Sciences, Subcommission on the
651 Systematics of Igneous Rocks. Cambridge University Press

652 Lee W-J, Wyllie P.J. 1994. Experimental Data Bearing on Liquid Immiscibility, Crystal
653 Fractionation, and the Origin of Calciocarbonatites and Natrocarbonatites. ~International
654 Geology Review, 36 797–819

655 Lee W-J, Wyllie P.J. 1997. Liquid immiscibility between nephelinite and carbonatite
656 from 1.0 to 2.5 GPa compared with mantle melt compositions. Contributions to Mineralogy
657 and Petrology 127, 1–16

658 Lee W-J, Wyllie P.J. 1998. Processes of crustal carbonatite formation by liquid
659 immiscibility and differentiation, elucidated by model systems. Journal of Petrology 39,
660 2005–2013

661 Loges, A., Migdisov, A. A., Wagner, T., Williams-Jones, A. E., and Markl, G. 2013.
662 An experimental study of the aqueous solubility and speciation of Y (III) fluoride at
663 temperatures up to 250 C. Geochimica et Cosmochimica Acta 123, 403–415

664 Macdonald R., Crossley, R., Waterhouse, K.S., 1983. Karroo basalts of southern
665 Malawi and their regional petrogenetic significance. Mineralogical Magazine 47, 281–289

666 Mariano, A. N. 1989. Nature of economic mineralization in carbonatites and related
667 rocks, pp. 149–176. In K. Bell (ed.), Carbonatites: genesis and evolution. Unwin Hyman,
668 London

669 McDonough, W., Sun, S., 1995. The composition of the Earth. Chemical Geology
670 120, 223–253

671 Nadeau, O., Cayer, A., Pelletier, M., Stevenson, R., Jébrak, M., 2015. The
672 Paleoproterozoic Montviel carbonatite-hosted REE–Nb deposit, Abitibi, Canada: Geology,
673 mineralogy, geochemistry and genesis. Ore Geology Reviews, 67, 314–335

674 Ngwenya, B.T., 1994. Hydrothermal rare earth mineralisation in carbonatites of the
675 Tundulu complex, Malawi: processes at the fluid/rock interface. Geochimica et
676 Cosmochimica Acta 58, 2061–2072

677 Rankin, A. 2005. Carbonatite-associated rare metal deposits: composition and
678 evolution of ore-forming fluids—the fluid inclusion evidence. Geological Association of
679 Canada, Short Course Notes 17:299–314

680 Snelling, N., 1966. Age determination unit. Report of the Overseas Geological Survey
681 p.p. 53

682 Soman, A., Geisler, T., Tomaschek, F., Grange, M., Berndt, J., 2010. Alteration of
683 crystalline zircon solid solutions: a case study on zircon from an alkaline pegmatite from
684 Zomba–Malosa, Malawi. Contributions to Mineralogy and Petrology 160, 909–930

685 Thomas, R.J., Jacobs, J., Horstwood, M.S.A., Ueda, K., Bingen, B., Matola, R. 2010.
686 The Mecuburi and Alto Benfica Groups, NE Mozambique: Aids to unravelling ca. 1 and 0.5
687 Ga events in the East African Orogen. Precambrian Research 178, 72–90

688 Thompson, R., Smith, P., Gibson, S., Mattey, D., Dickin, A., 2002. Ankerite
689 carbonatite from Swartbooisdrif, Namibia: the first evidence for magmatic ferrocarbonatite.
690 Contributions to Mineralogy and Petrology 143, 377–396

691 Wall, F., Barreiro, B.A., Spiro, B., 1994. Isotopic evidence for late-stage processes in
692 carbonatites: rare earth mineralization in carbonatites and quartz rocks at Kangankunde,
693 Malawi. Mineralogical Magazine, 58A, 951–952

694 Wall, F. Mariano, A. 1996. Rare earth minerals in carbonatites: a discussion centred
695 on the Kangankunde Carbonatite, Malawi, pp. 193–226. In A. Jones, F. Wall, and C. T.
696 Williams (eds.), Rare Earth Minerals: Chemistry Origin and Ore Deposits pp. 193–226.
697 Chapman and Hall, London

698 Wall, F., Zaitsev, A., 2004. Rare earth minerals in Kola carbonatites. In F. Wall and
699 A. Zaitsev (eds.), Phoscorites and carbonatites from mantle to mine: the key example of the
700 Kola alkaline province. Mineralogical Society, London

701 Wallace, M.E., Green, D.H., 1988. An experimental determination of primary
702 carbonatite magma composition. Nature, 335, 343–346

703 Woolley, A., 1991. The Chilwa Alkaline Igneous Province of Malawi: A review. In
704 Kampunzu, A.B., and Lubala, R.T., (Eds) Magmatism in Extensional Structural Settings: the
705 Phanerozoic African Plate. P.p. 377–409, Springer-Verlag, Berlin.

706 Woolley, A., 2001. Alkaline rocks and carbonatites of the World. Part 3: Africa. The
707 Geological Society. London, 372 pp

708 Woolley, A., Garson, M., 1970. Petrochemical and tectonic relationship of the Malawi
709 carbonatite-alkaline province and the Lupata-Lebombo volcanics, pp. 237–262. In G. I.
710 Clifford, T.N. (ed.), African Magmatism and Tectonics. Edinburgh, Oliver and Boyd

711 Woolley, A., Kempe, D., 1989. Carbonatites: nomenclature, average chemical
712 compositions, and element distribution. In K. Bell (ed.), Carbonatites: genesis and evolution.
713 Unwin Hyman, London, pp 1–14

714 Woolley, A., Bevan, J.C., Elliott, C.J., 1979. The Karroo dolerite dykes of southern
715 Malawi and their regional geochemical implications. Mineralogical Magazine, 43, 487–495.

716 Woolley, A., Platt, R.G., Eby, G.N., 1996. Aluminous alkali pyroxenes in nepheline
717 syenites from Malawi: mineralogical response to metamorphism/metasomatism in alkaline
718 rocks. The Canadian Mineralogist, 34, 423–434.

719 Xu, C., Kynicky, J., Chakhmouradian, A. R. Campbell, I. H., Charlotte, M. A., 2010
720 Trace-element modelling of the magmatic evolution of rare-earth-rich carbonatite from the
721 Miaoya deposit, central china. Lithos118, 145–155

722 Xu, C., Kynicky, J., Chakhmouradian, A.R., Li, X., Song, W., 2015 A case example of
723 the importance of multi-analytical approach in deciphering carbonatite petrogenesis in South
724 Qinling orogen: Miaoya rare-metal deposit, central China. Lithos 227, 107–121

List of Tables

Table 1. *Nomenclature of the carbonatite types at Songwe Hill. Use of the field ID and grouping is maintained throughout the manuscript*

Group	Field ID	Geochemical name (Gittins & Harmer, 1997)	Other names
C1	Calcite carbonatite	Calciocarbonatite	Sövite
C2	Calcite carbonatite	Calciocarbonatite	Alvikite
C3	Ferroan calcite carbonatite	Ferruginous calciocarbonatite	Ferrocarbonatite
N/A	Apatite-fluorite veins		
N/A	Mn-Fe-veins		Rødberg

729 **Table 2.** *Average whole-rock compositions for the different rock types at the Songwe Hill*

730 *carbonatite, plus two outlier apatite-fluorite-vein samples from Chenga Hill*

Sample	**Fenite**	**Calcite carbonatite**	**Ferroan calcite carbonatite**	**Mn-Fe-veins**	**Ap-Fl-veins**	**Chenga Hill**	
(Wt. %)	**Avg. (n=421)**	**Avg. (n=145)**	**Avg. (n=30)**	**Avg. (n=34)**	**Avg. (n=20)**	**T0178**	**T0134**
SiO_2	29.92	1.53	1.03	1.98	1.47	22.68	47.70
TiO_2	0.66	0.19	0.15	0.17	0.43	0.82	1.63
Al_2O_3	10.89	0.70	0.73	0.98	1.46	4.29	14.19
FeO	11.2	10.81	15.58	22.95	17.44	7.35	8.71
MnO	1.48	1.93	3.35	4.69	2.61	1.29	1.03
MgO	1.51	1.96	2.73	0.39	4.12	1.13	0.17
CaO	14.69	37.15	31.10	30.52	28.52	28.4	3.64
K_2O	6.65	0.43	0.19	0.38	0.34	2.75	9.2
P_2O_5	1.19	2.43	3.85	2.95	6.83	9.17	3.05
S	0.42	0.61	0.73	0.28	0.77	0.13	bd
SrO	0.75	2.07	2.78	0.55	0.54	0.48	0.13
Nb_2O_5	0.14	0.19	0.21	0.13	0.10	0.04	0.04
LOI (1000°C)	15.49	34.87	28.73	25.28	na	na	na
Total	94.99	94.85	91.21	91.09	63.93	77.99	89.33
(ppm)							
Be	13	2.7	4.1	4.4	na	na	na
Cr	5.5	0.7	5.6	3.6	na	na	na
Ga	5.8	12	0.3	9.3	bd	10	38
Hf	5.8	0.8	2.0	1.7	4.1	24	15
Li	8.5	3.4	5.4	4.2	na	na	na
Sc	0.2	2.0	20	14	na	na	na
Sn	6.5	2.7	3.9	2.6	na	na	na
Ta	19	1.3	0.8	1.4	na	na	na
Th	270	280	370	420	370	380	350
U	19	11	7.7	11	9.8	28	11
V	110	140	140	200	na	na	na
W	14	8.6	15	9.1	na	na	na
Zr	361.1	37.3	101.1	87.8	223.6	1293	819

La	1600	3500	9200	5300	3200	860	1300
Ce	2800	6700	13400	9100	6600	1300	1900
Pr	290	720	1400	940	760	120	190
Nd	970	2400	4100	2900	2700	420	620
Sm	150	340	480	380	400	100	100
Eu	44	95	120	100	120	55	37
Gd	110	220	280	240	280	250	130
Tb	14	29	34	31	39	79	26
Dy	62	140	150	150	210	560	150
Ho	9.9	24	24	24	39	100	28
Er	23	57	54	54	110	260	66
Tm	2.8	7.3	6.6	6.7	15	31	8.0
Yb	17	41	35	38	85	170	45
Lu	2.2	5.2	4.5	5.0	11	21	5.5
Y	250	610	590	590	1000	3000	740

bd: below detection limits, na: not analysed For full dataset see **Supplementary Table 2.**

NB: Ba and Na not analysed owing to preparation as Na-peroxide fusion

731

732 **Table 3.** *Laser-ablation U–Pb ages*

Sample	Rock type	Regression intercept age (Ma), 2σ	MSWD, n	Regression uncertainty with σ_{sys} (2σ Ma)
T0208 (Session 1)	C1	129.5 ± 3.3	1.9, n= 7	4.3
T0206 (Session 1)	C1	131.8 ± 2.5	4.4, n= 11	3.7
T0206 (Session 2)	C1	132.9 ± 1.1	7.5, n= 34	3.0
T0206 (Session 3)	C1	137.3 ± 1.0	1.8, n= 11	3.1
U4913 (Session 1)	Nepheline syenite	137.5 ± 1.5	3.6, n= 18	3.3
U4913 (Session 3)	Nepheline syenite	131.7 ± 0.9	6.1, n= 43	2.9
T0225 (Session 3)*	C2	135.6 ± 2.5	1.9, n= 5	3.8

733 *Excluding one point from regression

734

List of Figures

Figure 1: Map of the Chilwa Alkaline Province, adapted from Woolley (2001). Included for reference are the ages of the major carbonatites, from: Snelling (1966) [Kangankunde, Chilwa Island, Tundulu], Wall et al., (1994) [Kangankunde], and Eby et al. (1995) [Chilwa Island].

Figure 2: Geological map of Mauze and Songwe (A) and of carbonatite types at Songwe (B). Drill holes from which samples were taken are indicated. For the complete geological map, and all drill hole collars, see Croll et al. (2014). Grid system is UTM 36S, WGS1984 datum. Maps redrawn after Garson and Walshaw (1969) and Croll et al. (2014).

Figure 3: Field photos of the major lithologies at Songwe (A) contact breccia on Chenga Hill displaying decreasing degrees of fenitization between the edges and cores of clasts; (B) Grey C2 calcite carbonatite incorporating clasts of fenite and cross-cut by small Mn-Fe-veins; (C) Carbonate-rich breccia, incorporating two different types of calcite carbonatite: earlier C1 calcite carbonatite, and later C2 calcite carbonatite; (D) Contact between (C3) Ferroan calcite carbonatite and C2 calcite carbonate in drill core (PX003, 16 m depth); (E) Ferroan calcite carbonatite breccia with clasts of C1 calcite carbonatite and fenite; (F) Example of a road-cut with extensive alteration of Fe-rich rock to hematite, goethite, wad and limonite. Hammer head is approximately 10 cm.

Figure 4: Cathodoluminescence (B–D, H) and back-scattered electron (E–G) images of Songwe carbonatites. (A) Large euhedral apatite, zircon and pyrite in C1 calcite carbonatite; (B) apatite bands in C2 calcite carbonatite; (C) vugs of synchysite, baryte and strontianite in C2 calcite carbonatites; (D) truncation of an apatite stringer by a REE-fluorcarbonate-bearing assemblage in C3 carbonatites; (E) partially fragmented apatite in a matrix of strontianite and fluorcarbonates in C3 carbonatites; and, (F) apatite and fluorite in an apatite-fluorite vein sample.

Figure 5: Back-scattered electron images of zircon from Songwe carbonatite. (A–B) Unzoned subhedral zircons in C1 carbonatite; (C) corroded zircon from C2 carbonatite; (D–E) zoned fractured zircon in C1 carbonatite Circles approximate ablation pit locations. Labels correspond to results in Supplementary Table 5.

Figure 6: Ternary carbonatite classification diagrams after Gittins and Harmer (1997), and Woolley and Kempe (1989). The trends caused by increasing contents of minerals that can affect the carbonatite composition on this diagram are indicated.

Figure 7: Whole-rock data from carbonatite, Mn-Fe- veins and apatite-fluorite veins from Songwe. (A) LOI represents a close approximation of CO_2. Grey lines equate to mixing lines between pure calcite (bottom-right) and various Fe-phases indicated on the graph. These are simple plots of binary mixing and are not intended to be wholly representative of the composition of the samples. Lines in all other figures are to indicate the main interpreted trends in the data. NB, C1 samples were too scarce for whole-rock analysis.

Figure 8: Average distributions of the REE in Songwe carbonatites, Mn-Fe veins and apatite-fluorite veins normalised to (A) chondrite and (B) C2 carbonatite. Symbols same as for Figure 7.

Figure 9: Example Tera-Wasserburg plot of Songwe sample T0206 (session 3). See Table 3 for other U–Pb ages and supplementary Table 5 for dates.

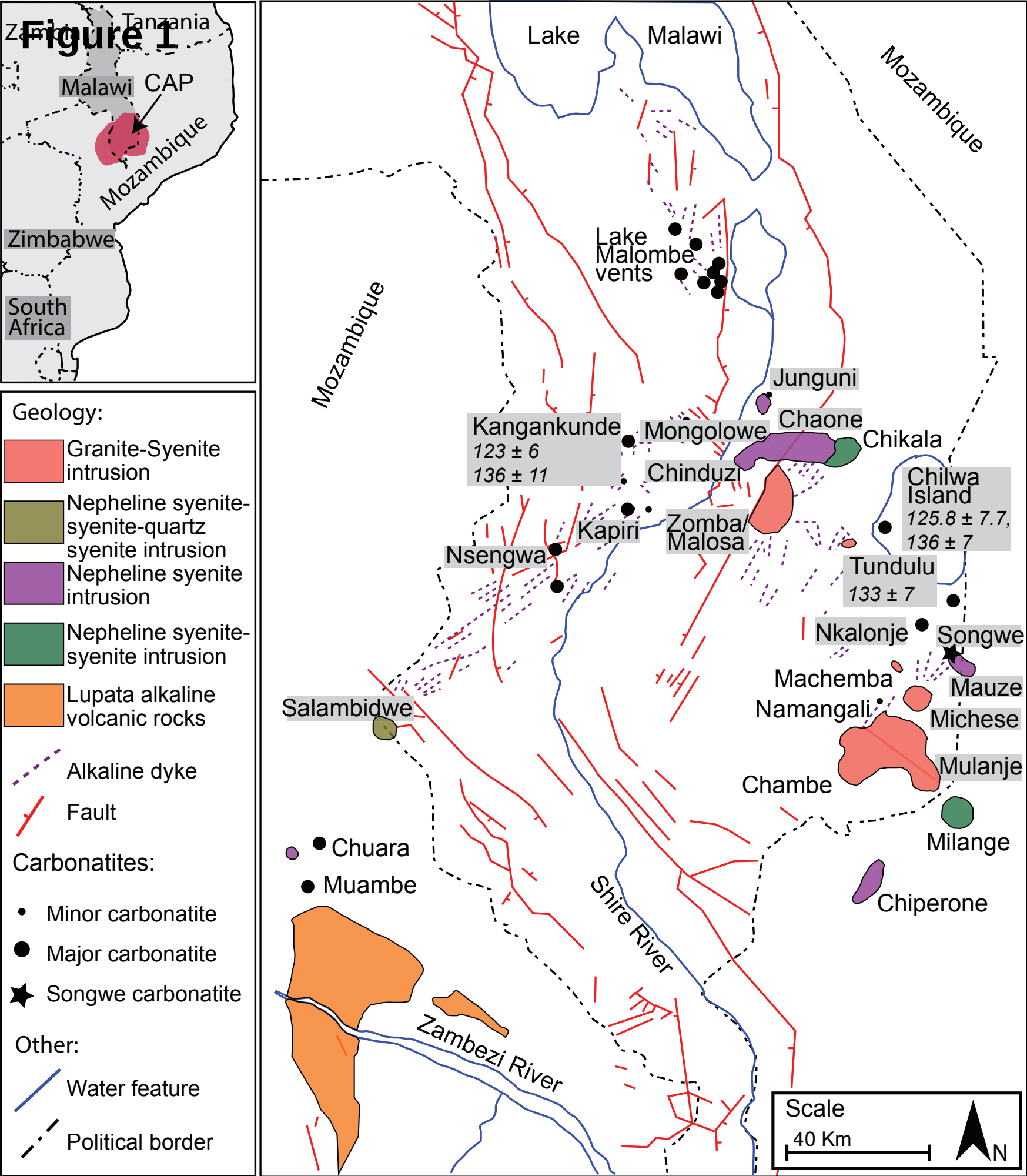
Figure 1
Zambia
Tanzania
Malawi
CAP
Mozambique
Zimbabwe
South Africa
Geology:
Granite-Syenite intrusion
Nepheline syenite-syenite-quartz syenite intrusion
Nepheline syenite intrusion
Nepheline syenite-syenite intrusion
Lupata alkaline volcanic rocks
Alkaline dyke
Fault
Carbonatites:
Minor carbonatite
Major carbonatite
Songwe carbonatite
Other:
Water feature
Political border
Lake Malawi
Mozambique
Lake Malombe vents
Junguni
Kangankunde
123 ± 6
136 ± 11
Mongolowe
Chaone
Chikala
Chinduzi
Chilwa Island
125.8 ± 7.7,
136 ± 7
Kapiri
Zomba/ Malosa
Nsengwa
Tundulu
133 ± 7
Nkalonje
Songwe
Machemba
Mauze
Namangali
Michese
Salambidwe
Chambe
Mulanje
Milange
Chuara
Muambe
Chiperone
Shire River
Zambezi River
Scale
40 Km
N

Figure 2

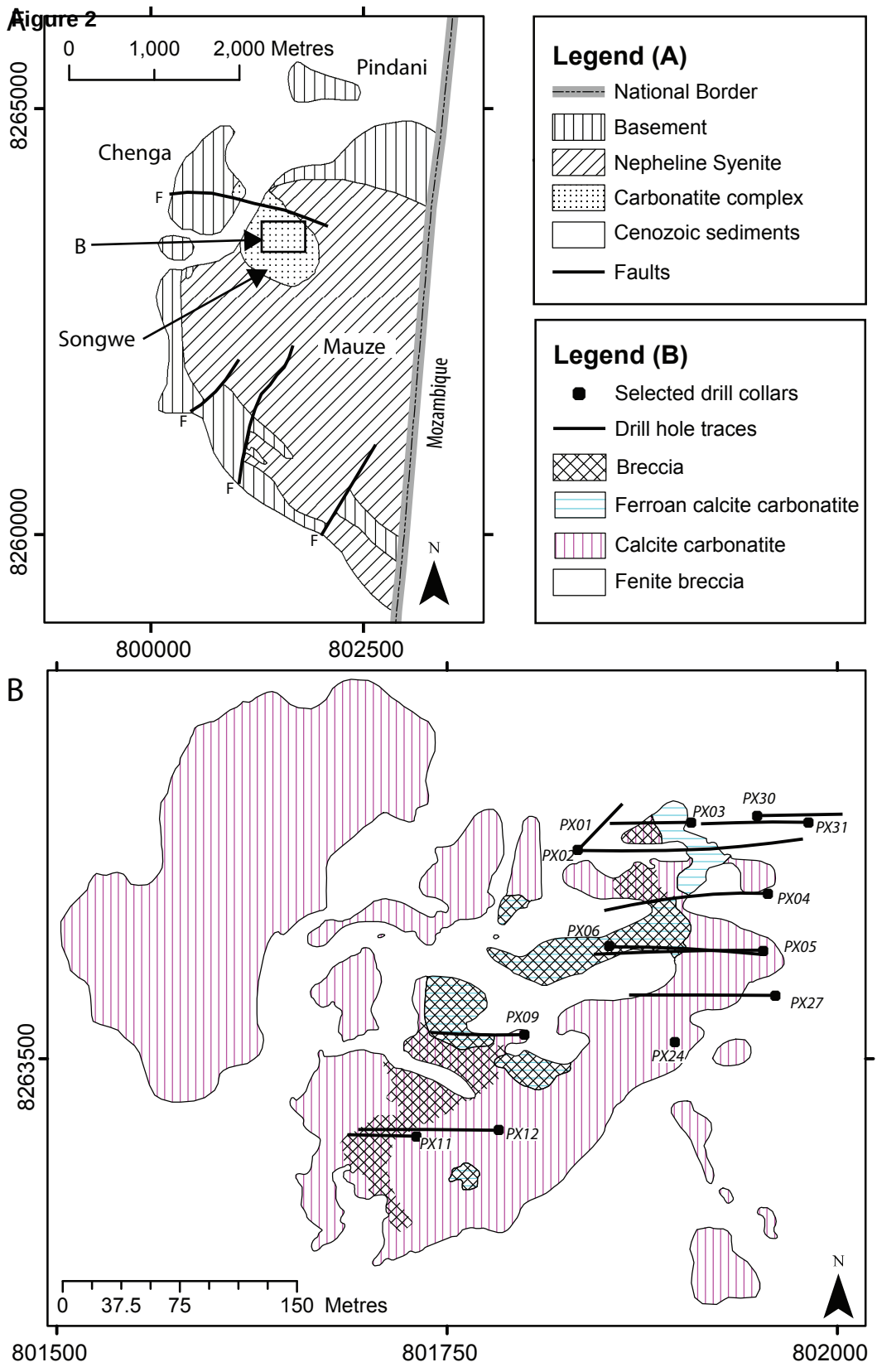
A
0
1,000
2,000 Metres
Pindani
Chenga
F
B
Songwe
Mauze
Mozambique
F
F
F
N
8265000
8260000
800000
802500
Legend (A)
National Border
Basement
Nepheline Syenite
Carbonatite complex
Cenozoic sediments
Faults
Legend (B)
Selected drill collars
Drill hole traces
Breccia
Ferroan calcite carbonatite
Calcite carbonatite
Fenite breccia
B
PX01
PX02
PX03
PX30
PX31
PX04
PX06
PX05
PX27
PX09
PX24
PX11
PX12
0
37.5
75
150 Metres
N
8263500
801500
801750
802000

Figure 3

Click here to download high resolution image

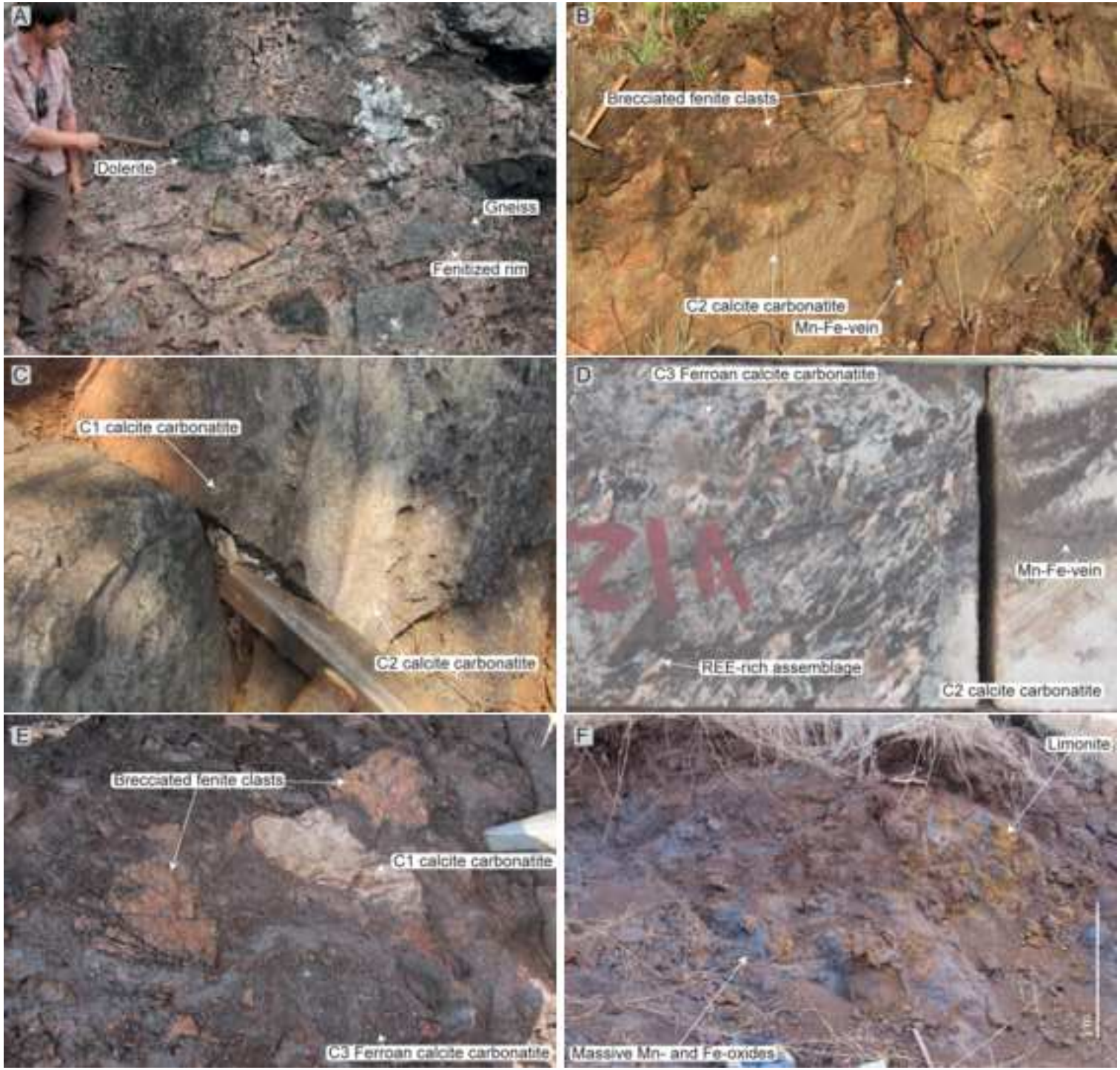

Figure 4

Click here to download high resolution image

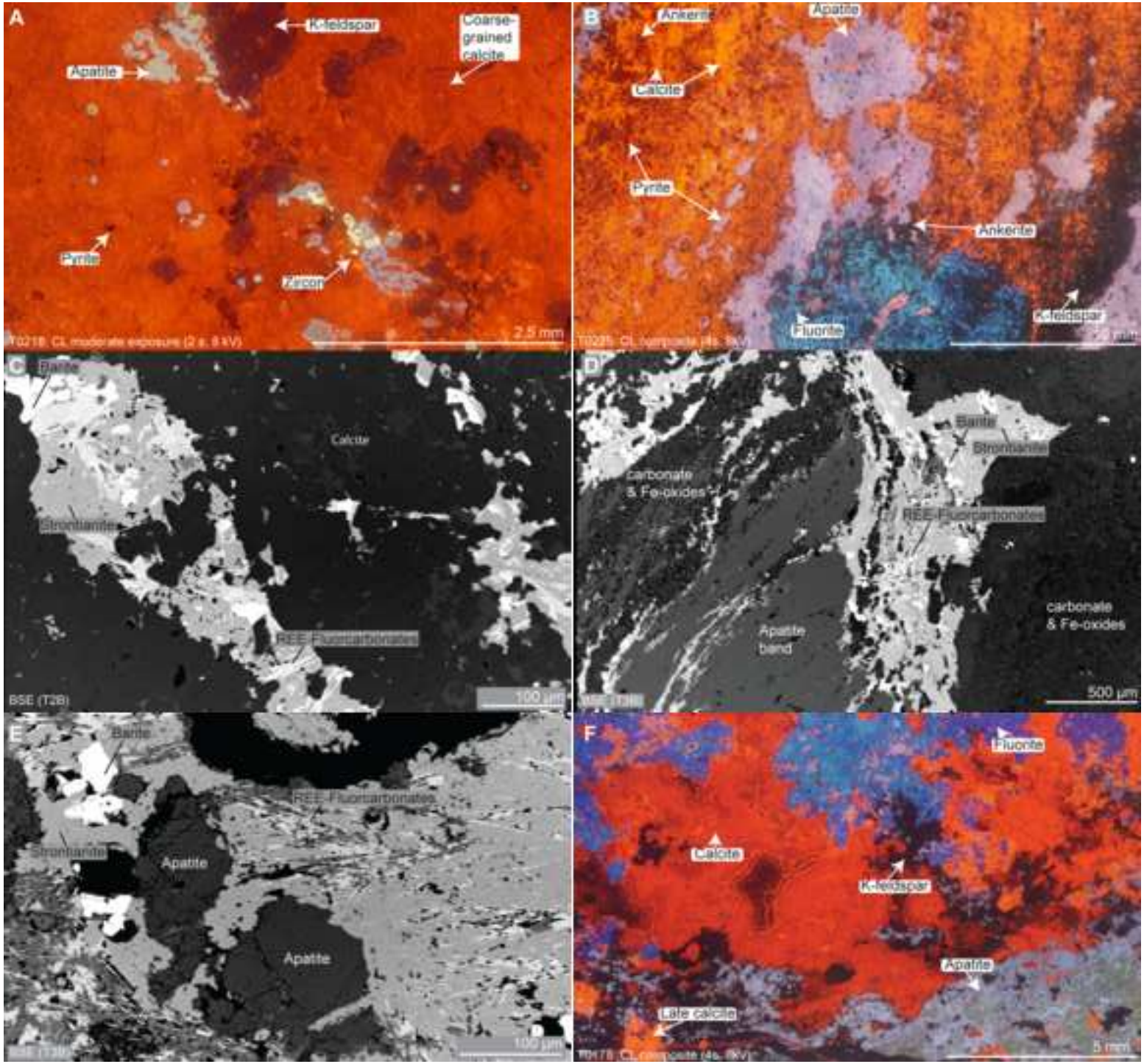

Figure 5

Click here to download high resolution image

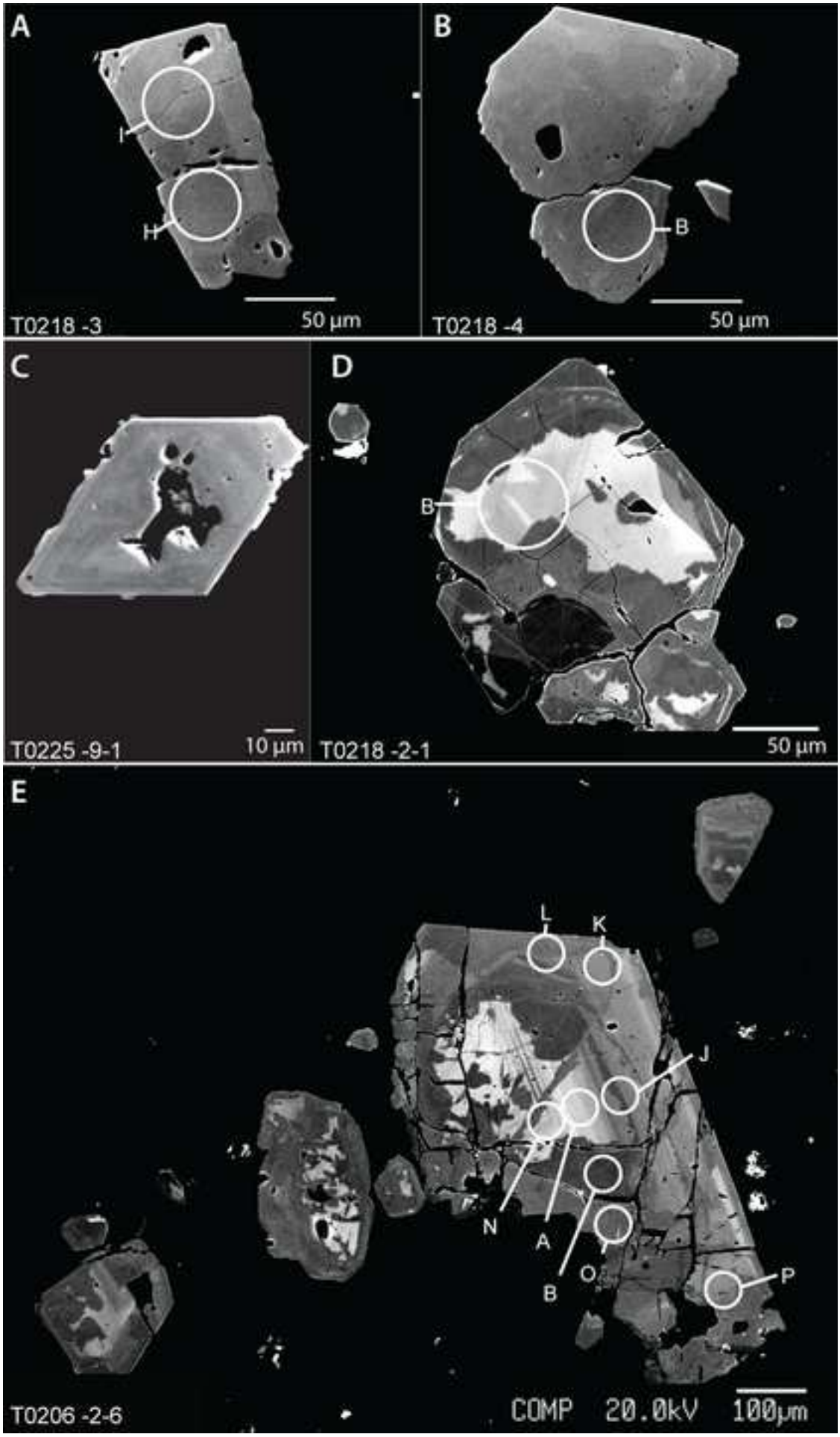

Figure 6

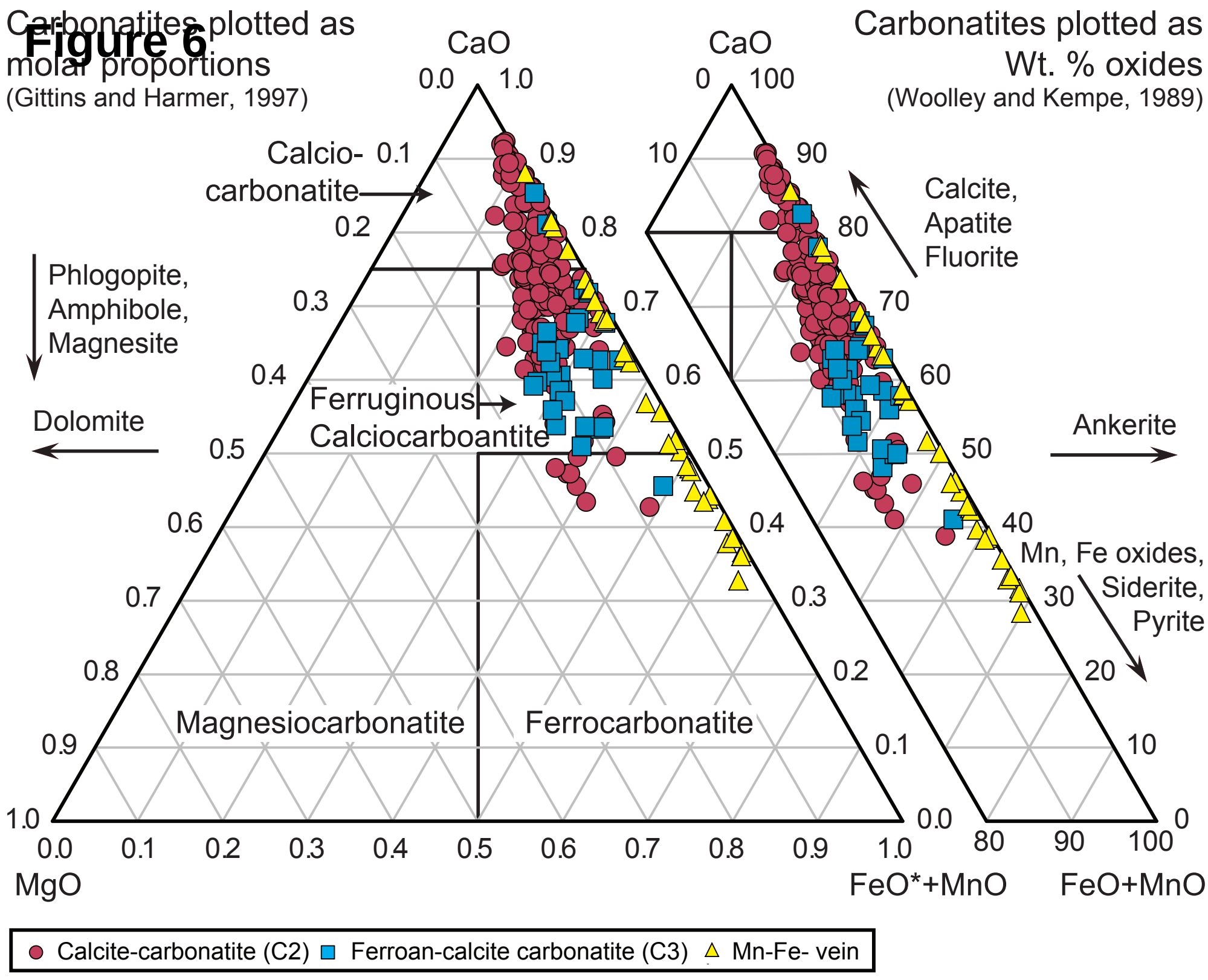
Carbonatites plotted as molar proportions
(Gittins and Harmer, 1997)
Carbonatites plotted as Wt. % oxides
(Woolley and Kempe, 1989)
CaO
MgO
FeO*+MnO
FeO+MnO
Calcio-carbonatite
Ferruginous Calciocarboantite
Magnesiocarbonatite
Ferrocarbonatite
Phlogopite, Amphibole, Magnesite
Dolomite
Calcite, Apatite Fluorite
Ankerite
Mn, Fe oxides, Siderite, Pyrite
Calcite-carbonatite (C2)
Ferroan-calcite carbonatite (C3)
Mn-Fe- vein

Figure 7

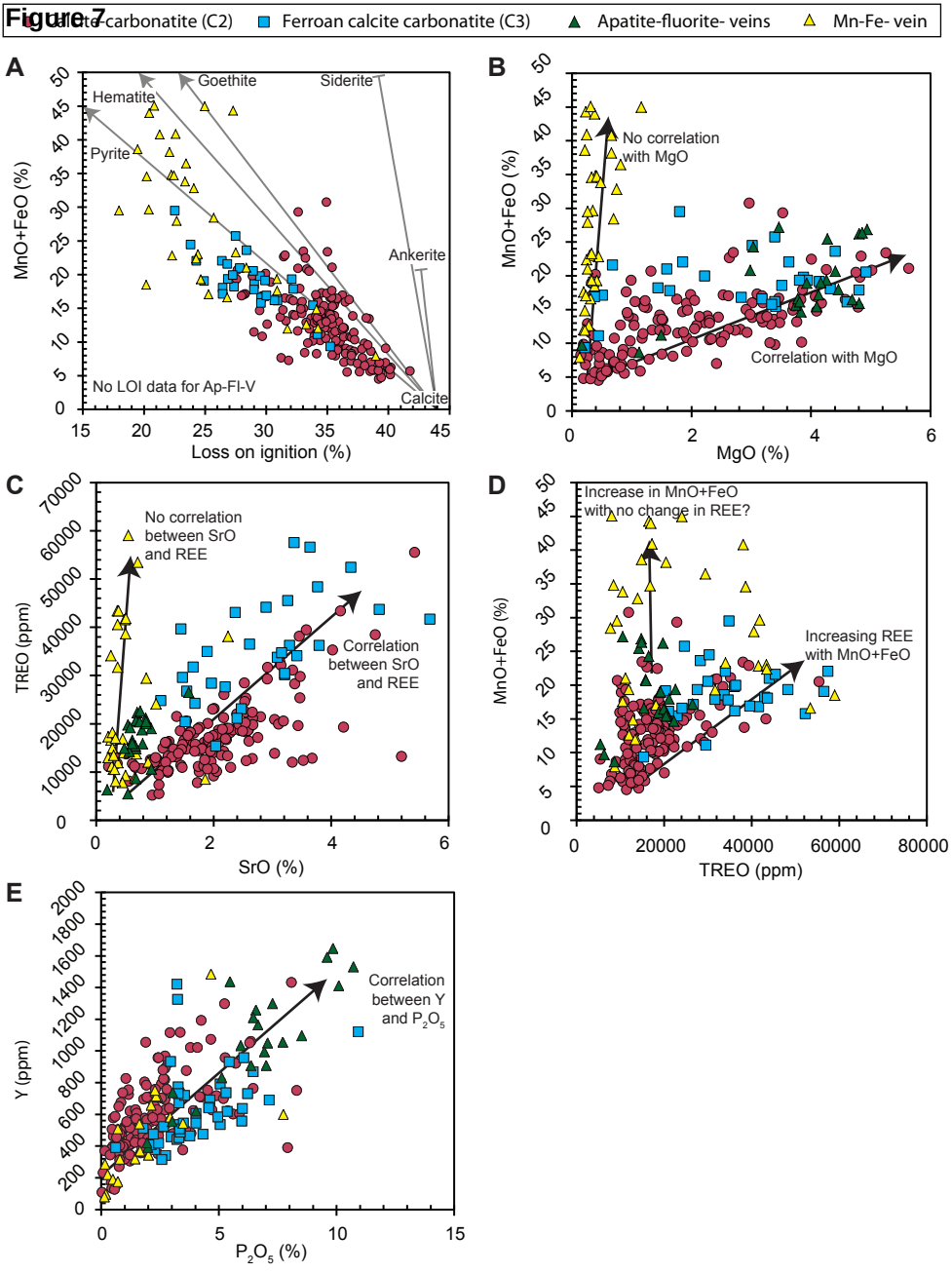
Ferroan calcite carbonatite (C2)
Ferroan calcite carbonatite (C3)
Apatite-fluorite- veins
Mn-Fe- vein
A
Hematite
Goethite
Siderite
Pyrite
Ankerite
Calcite
No LOI data for Ap-Fl-V
MnO+FeO (%)
Loss on ignition (%)
B
No correlation with MgO
Correlation with MgO
MnO+FeO (%)
MgO (%)
C
No correlation between SrO and REE
Correlation between SrO and REE
TREO (ppm)
SrO (%)
D
Increase in MnO+FeO with no change in REE?
Increasing REE with MnO+FeO
MnO+FeO (%)
TREO (ppm)
E
Correlation between Y and P2O5
Y (ppm)
P2O5 (%)

Figure 8

A
Concentration (chondrite normalised)
100000
10000
1000
100
La
Ce
Pr
Nd
(Pm)
Sm
Eu
Gd
Tb
Dy
Y
Ho
Er
Tm
Yb
Lu
B
Concentration (Songwe C2 carbonatite normalised)
3.0
2.5
2.0
1.5
1.0
0.5
La
Ce
Pr
Nd
(Pm)
Sm
Eu
Gd
Tb
Dy
Y
Ho
Er
Tm
Yb
Lu

Figure 9

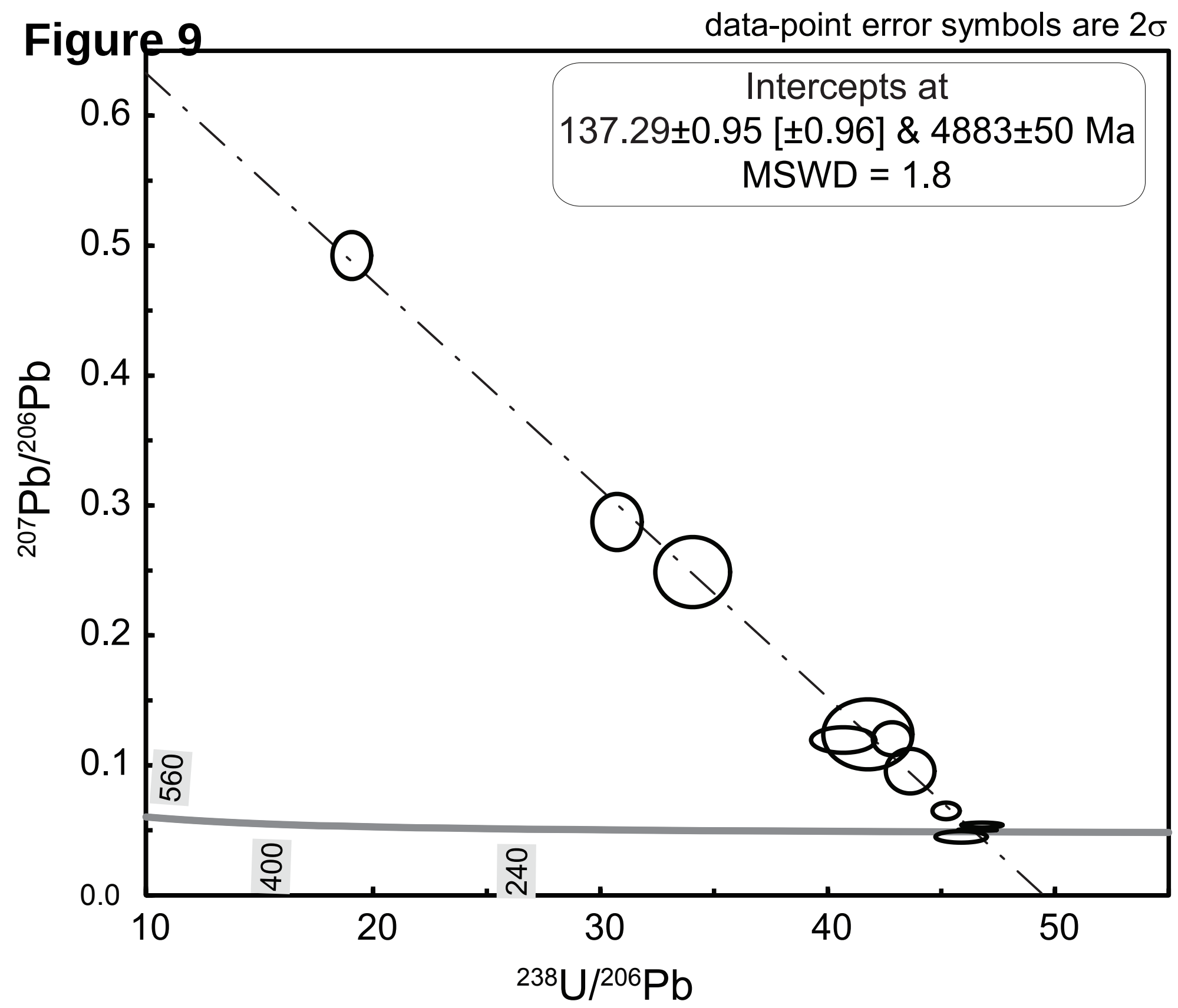
data-point error symbols are 2σ
Intercepts at
137.29±0.95 [±0.96] & 4883±50 Ma
MSWD = 1.8
0.6
0.5
0.4
0.3
0.2
0.1
0.0
207Pb/206Pb
560
400
240
0
10
20
30
40
50
238U/206Pb